Relativistic Electron Energy Loss and Electron-Induced Photon Emission in Inhomogeneous Dielectrics

F. J. García de Abajo

Departamento de Ciencias de la Computación e Inteligencia Artificial, Facultad de Informática, and Departamento de Física de Materiales, Facultad de Química, Universidad del Pais Vasco, San Sebastián, Spain

A. Howie

Cavendish Laboratory, Madingley Road, Cambridge CB3 OHE, United Kingdom

(Received 21 January 1998)

Electron loss and electron-induced photon-emission probabilities are calculated near arbitrarily shaped dielectrics described by frequency-dependent response functions. The exact solution of Maxwell's equations is reduced to self-consistent equations involving integrals over the interfaces. The particular case of axially symmetric interfaces of arbitrary shape is discussed in detail. Photon-emission probabilities are shown to be of the same order of magnitude as loss probabilities in some cases, suggesting the possibility of measuring electron-induced radiation as a new microscopy technique. [S0031-9007(98)06300-5]

PACS numbers: 73.20.Mf, 41.20.Jb, 61.16.Bg, 84.90.+a

Scanning transmission electron microscopy (STEM) can perform electron energy loss spectroscopy on the nanometer scale. The relatively intense valence-loss spectral region $\Delta E = \hbar\omega \leq 50$ eV can be interpreted using the classical response theory based on the complex, frequency-dependent dielectric function $\epsilon(\omega)$ for each component of the specimen structure. In the nonrelativistic approximation, analytical eigenmode and stopping power solutions for simple shapes such as planes [1,2], cylinders [3], or spheres [4,5] have proved useful and, for more complex geometries, can be supplemented by a numerical, boundary-charge approach [6–9]. These nonrelativistic calculations neglect retardation effects, which become significant in structures of characteristic dimension $a > c/w$, and also ignore all radiative losses, including transition and Cherenkov radiation. Relativistic analytical solutions, however, if available at all, are much more complicated even for slabs or planes [10,11].

Retardation effects can be incorporated in full three-dimensional computations. Purcell and Pennypacker's method [12] of filling each part of the dielectric medium with an array of coupled dipoles has been applied to study the optical properties of dielectric grains as well as to both isolated and interacting spheres [13,14]. Recently, Pendry *et al.* [15] have developed a new numerical method of solving Maxwell's equations for the study of photonic band structures.

Here, for structures of arbitrary shape, we present a new approach to the computation of energy loss and electron-induced photon-emission spectra based on the numerical solution of Maxwell's equations by the boundary element method [16]. A detailed study of the case of small spheres shows that, even outside the familiar Cherenkov or transition radiation regimes, photon-emission probabilities can be a significant fraction of total loss probabilities, suggesting the possibility of detecting the induced radiation to derive information on the target.

The electric and magnetic fields in a nonmagnetic inhomogeneous material are conveniently expressed in terms of scalar and vector potentials ϕ and $\mathbf{A}$ as $\mathbf{H} = \nabla \times \mathbf{A}$ and $\mathbf{E} = \frac{i\omega}{c}\mathbf{A} - \nabla\phi$, respectively, where the Lorentz gauge condition $\nabla \cdot \mathbf{A} - \frac{i\omega}{c}\epsilon\phi = 0$ has been adopted, ϵ is the space and frequency-dependent local dielectric function [atomic units (a.u.) will be used unless otherwise specified]. Then, the Maxwell equations reduce to

$$(\nabla^2 + k^2\epsilon)\phi = -4\pi(\rho/\epsilon + \sigma_s), \tag{1a}$$

$$(\nabla^2 + k^2\epsilon)\mathbf{A} = -\frac{4\pi}{c}(\mathbf{j} + \mathbf{m}), \tag{1b}$$

where $k = \omega/c$, $\sigma_s = \frac{1}{4\pi}\mathbf{D} \cdot \nabla\frac{1}{\epsilon}$, $\mathbf{m} = -\frac{i\omega}{4\pi}\phi\nabla\epsilon$, and ρ ($\mathbf{j}$) is the external charge (current) density.

Focusing on an abrupt interface separating two different media described by dielectric functions ϵ_j, $j = 1, 2$, the electromagnetic fields find their sources in both the external perturbation and the polarization charges and currents induced on the interface, σ_s and $\mathbf{m}$, as can be seen in Eqs. (1). Therefore, the fields must result from the propagation of these sources by means of Green functions $G_j(r) = \exp(ik_j r)/r$ appropriate for each separate medium, where $k_j = k\sqrt{\epsilon_j(\omega)}$ and the square root is chosen such that k_j lies in the upper complex plane in order to guarantee that the fields vanish at infinity. More precisely, the potentials inside medium j read

$$\begin{bmatrix} \phi(\mathbf{r}) \\ \mathbf{A}(\mathbf{r}) \end{bmatrix} = \int d\mathbf{r}'\, G_j(|\mathbf{r} - \mathbf{r}'|) \begin{bmatrix} \rho(\mathbf{r}')/\epsilon(\mathbf{r}', \omega) \\ \mathbf{j}(\mathbf{r}')/c \end{bmatrix} + \int_S d\mathbf{s}\, G_j(|\mathbf{r} - \mathbf{s}|) \begin{bmatrix} \sigma_j(\mathbf{s}) \\ \mathbf{h}_j(\mathbf{s}) \end{bmatrix}, \tag{2}$$

 0031-9007/98/80(23)/5180(4)$15.00

where the additional integrals over the interface S are required partly to include the effects of the interface charges and currents noted above and partly to compensate for the discontinuity of the Green function at the interface. Actually, upon insertion of Eq. (2) into Eqs. (1), one finds that the former is the solution of the latter vanishing at infinity, provided the customary boundary conditions of the electromagnetic field are satisfied. Moreover, those boundary conditions determine σ_j and $\mathbf{h}_j$ for a given choice of the external source.

The continuity of the parallel electric field and the normal magnetic field at the interface is guaranteed by the continuity of the potentials, which in turn leads to

$$G_1\sigma_1 - G_2\sigma_2 = -(\varphi_1 - \varphi_2)\,, \tag{3a}$$

$$G_1\mathbf{h}_1 - G_2\mathbf{h}_2 = -(\mathbf{g}_1 - \mathbf{g}_2)\,, \tag{3b}$$

where

$$\begin{bmatrix} \varphi_j(\mathbf{s}) \\ f_j(\mathbf{s}) \end{bmatrix} = \int d\mathbf{r} \begin{bmatrix} 1 \\ \mathbf{n}_s \cdot \nabla_{\mathbf{s}} \end{bmatrix} G_j(|\mathbf{s} - \mathbf{r}|) \frac{\rho(\mathbf{r})}{\epsilon(\mathbf{r}, \omega)}\,, \tag{4}$$

and matrix notation has been adopted, so that interface coordinates $\mathbf{s}$ are used as matrix and vector indices, and matrix-vector products such as $G_j\sigma_j$ involve integration over the interface.

The continuity of the parallel magnetic field and the normal electric displacement leads to

$$H_1\mathbf{h}_1 - H_2\mathbf{h}_2 + p\mathbf{n}_s G_1\sigma_1 = -\mathbf{q}_1 + \mathbf{q}_2 - p\mathbf{n}_s\varphi_1\,, \tag{5a}$$

$$\frac{1}{ik}(\epsilon_1 H_1\sigma_1 - \epsilon_2 H_2\sigma_2) - \epsilon_1\mathbf{n}_s G_1 \cdot \mathbf{h}_1 + \epsilon_2\mathbf{n}_s G_2 \cdot \mathbf{h}_2 = \epsilon_1\left(\mathbf{n}_s \cdot \mathbf{g}_1 - \frac{f_1}{ik}\right) - \epsilon_2\left(\mathbf{n}_s \cdot \mathbf{g}_2 - \frac{f_2}{ik}\right), \tag{5b}$$

where $H_j(\mathbf{s} - \mathbf{s}') = \mathbf{n}_s \cdot \nabla_{\mathbf{s}} G_j(|\mathbf{s} - \mathbf{s}'|) \pm 2\pi\delta(\mathbf{s} - \mathbf{s}')$ (the sign is + for $j = 1$, and − for $j = 2$), $p = ik(\epsilon_2 - \epsilon_1)$,

$$\begin{bmatrix} \mathbf{g}_j(\mathbf{s}) \\ \mathbf{q}_j(\mathbf{s}) \end{bmatrix} = \frac{1}{c} \int d\mathbf{r} \begin{bmatrix} 1 \\ \mathbf{n}_s \cdot \nabla_{\mathbf{s}} \end{bmatrix} G_j(|\mathbf{s} - \mathbf{r}|)\, \mathbf{j}(\mathbf{r})\,, \tag{6}$$

and $\mathbf{n}_s$ is chosen to point towards medium 2.

Upon discretization of the surface integrals using N points, Eqs. (3)–(6) become a set $8N$ linear equations, which can be solved by direct numerical inversion in a time proportional to $512N^3$. A more efficient ($6N^3$) numerical procedure has been followed here consisting in separately manipulating operators such as G_j, which now become $N \times N$ matrices.

For simplicity, we have considered the case of axially symmetric, but otherwise arbitrarily shaped, dielectrics. This allows analytical evaluation of the azimuthal interface integrals, so that the number of points N is considerably reduced, though one has to sum over the azimuthal momentum number m. In the examples that follow, 50 points per object have been enough to reach convergence.

The loss probability Γ^{loss} for an electron moving with velocity $\mathbf{v}$ can be obtained from the induced electric field $\mathbf{E}^{\text{ind}}$ acting on the electron, whose sources are found in the auxiliary boundary charges and currents [see Eq. (2)]. One has

$$\Gamma^{\text{loss}}(\omega) = \frac{1}{\pi\omega} \int dt\, \text{Re}\{e^{-i\omega t}\mathbf{v} \cdot \mathbf{E}^{\text{ind}}[\mathbf{r}_e(t), \omega]\}\,, \tag{7}$$

where $\mathbf{r}_e(t)$ describes the electron trajectory.

Figure 1 shows the loss probability for an electron moving near a set of aligned spheres as shown in the insets. The results derived from the nonrelativistic theory (broken curves, obtained in the $c \to \infty$ limit) are compared with the fully relativistic results (solid curves). The Drude dielectric function $\epsilon(\omega) = 1 - \frac{\omega_p^2}{\omega(\omega + i\eta)}$ has been used to describe the target, with parameters appropriate for Al. The frequencies of the various loss peaks are characteristic of each target, and the electron velocity and trajectory determine the weight of each of them in the spectrum. Under the conditions considered in Fig. 1, typical of STEM, the lowest order m modes are emphasized. The figure illustrates how much they are influenced by relativistic effects for targets on the nanometer scale.

Previous nonrelativistic results for one [4] and two [5] spheres are fully reproduced using the present method. As a further test, the relativistic calculations of Fig. 2 for the isolated sphere have been compared with an analytical expression, which can be written as a sum over the contribu-

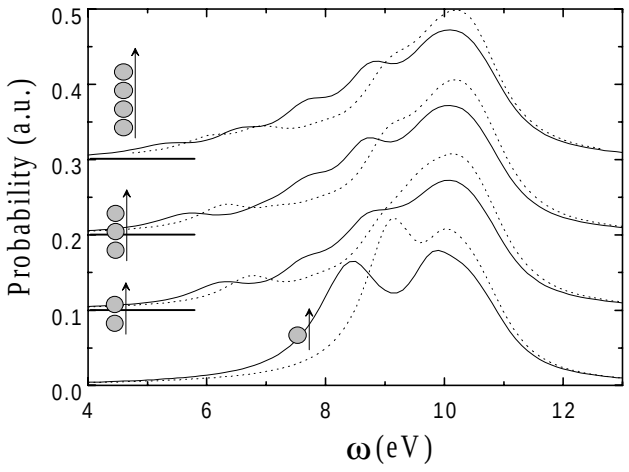

FIG. 1. Loss probability per unit energy range and per sphere for a 100-keV electron traveling in vacuum parallel to the axis of symmetry of a set of 1–4 aligned Al spheres and passing at 1 nm from their surfaces. Consecutive curves are shifted 0.1 a.u. upwards to improve readability. The spheres are described by the Drude dielectric function (see text) with $\omega_p = 15.8$ eV and $\eta = 1.06$ eV. The radius of the spheres is 10 nm. Contiguous spheres are separated by 1 nm. Solid (broken) curves correspond to the relativistic (nonrelativistic) theory. The total loss probability per sphere is ≈2.2% in all cases.

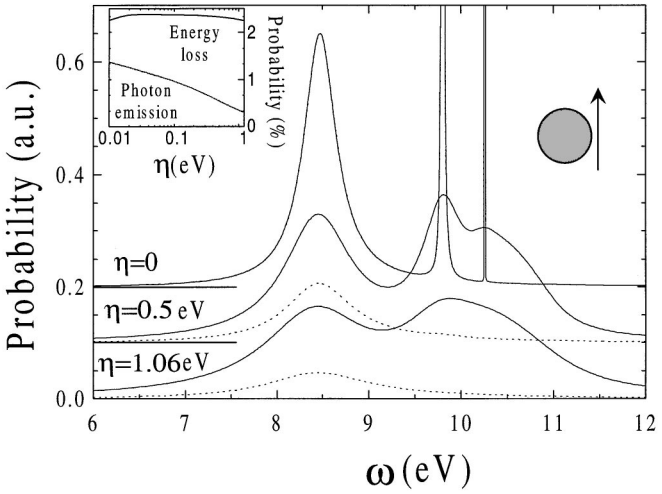

FIG. 2. Loss probability (solid curves) and photon-emission probability (broken curves) for a 100-keV electron passing at a distance of 1 nm from a sphere of radius 10 nm described by the Drude dielectric function with $\omega_p = 15.8$ eV and different values of the damping η (see labels). The inset shows the total probability as a function of damping.

tion of different multipoles. More precisely [17],

$$\Gamma^{\mathrm{loss}}(\omega) = \frac{1}{c\omega}\sum_{l=1}^{\infty}\sum_{m=-l}^{l} K_m^2\left(\frac{\omega b}{v\gamma}\right) \times [C_{lm}^{M}\,\mathrm{Im}\,\{t_l^{M}\} + C_{lm}^{E}\,\mathrm{Im}\,\{t_l^{E}\}], \quad (8)$$

where γ is the Lorentz relativistic contraction factor, C_{lm}^{M} and C_{lm}^{E} are positive constants that depend only on v/c, and $t_l^{\nu} = \sin\delta_l^{\nu}\exp(\delta_l^{\nu})$ are the magnetic and electric scattering matrices written in terms of the corresponding phase shifts [18] δ_l^{ν} for $\nu = M$ and $\nu = E$, respectively. The results of analytical and numerical calculations cannot be separated on the scale of Fig. 2 (solid curves).

The photon-emission probability Γ^{rad} has been obtained by dividing by ω the component of the Poynting vector normal to an arbitrarily large sphere centered at the sample. The emission increases with decreasing damping η and it coincides with the loss probability for real dielectric functions, in which case the medium cannot absorb any energy and the stopping of the electron goes entirely into radiation. This is shown in Fig. 2 (broken curves) for the case of an isolated sphere. Actually, for the isolated sphere, Γ^{rad} is given by Eq. (8) upon substitution of $|t_l^{\nu}|^2$ for $\mathrm{Im}\{t_l^{\nu}\}$ and it is easy to show explicitly that $\Gamma^{\mathrm{loss}} = \Gamma^{\mathrm{rad}}$ for real dielectric functions. The finite loss probability for $\eta = 0$ is due to the finite width of the natural oscillations of the sphere [19].

The emitted radiation is not subject to the Cherenkov condition for low-l modes [this follows from Eq. (8)], dominant in the case considered in Fig. 2. Rather, it is connected to the intrinsic finite width of the modes of the sphere. Nevertheless, even at 100 keV the radiative corrections for an isolated 10-nm sphere are quite significant (see inset in Fig. 2). The photon-emission probability and the loss probability are both of the same order of magnitude, making possible the direct detection of the electron-induced photon emission under study.

For a realistic finite damping η, the photon-emission probability presents the same features contained in the loss function, but some of them are nearly suppressed, as can be seen both in Fig. 2 for the isolated sphere and in the upper part of Fig. 3 for the same targets as in Fig. 1. The angular distributions of photons shown in the contour

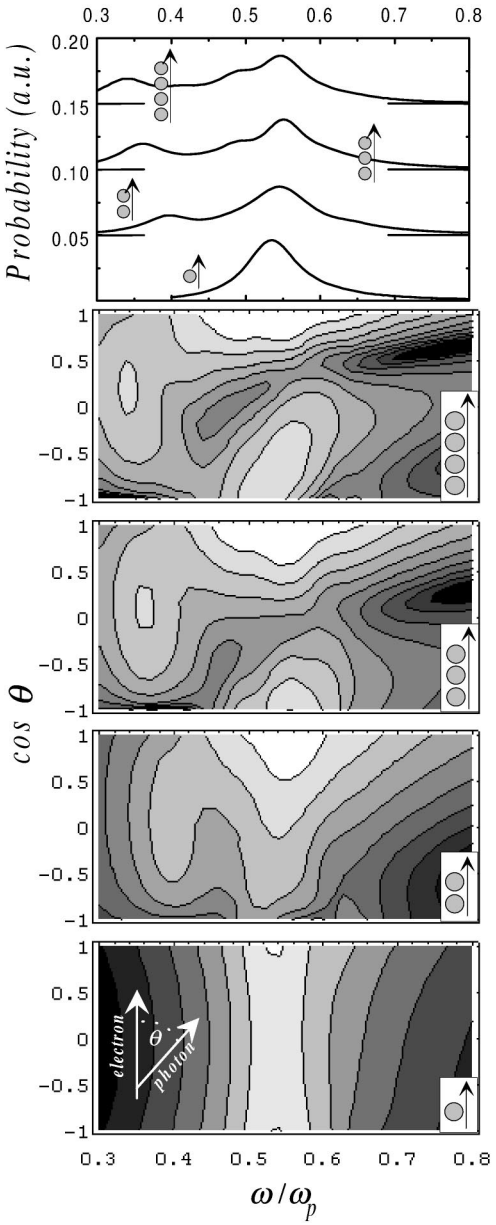

FIG. 3. Upper part: Photon-emission probability under the same conditions as in Fig. 1, except that the probability has not been divided by the number of spheres. Lower part: Contour plots showing the angle-resolved photon-emission probability averaged over azimuthal directions. The distance between consecutive contour curves corresponds to a factor of 2, starting from small values in the dark regions and reaching 0.005 a.u. per stereo radian in the curves limiting white areas. The total emission probability ranges from 0.32% (on sphere) to 0.42%.

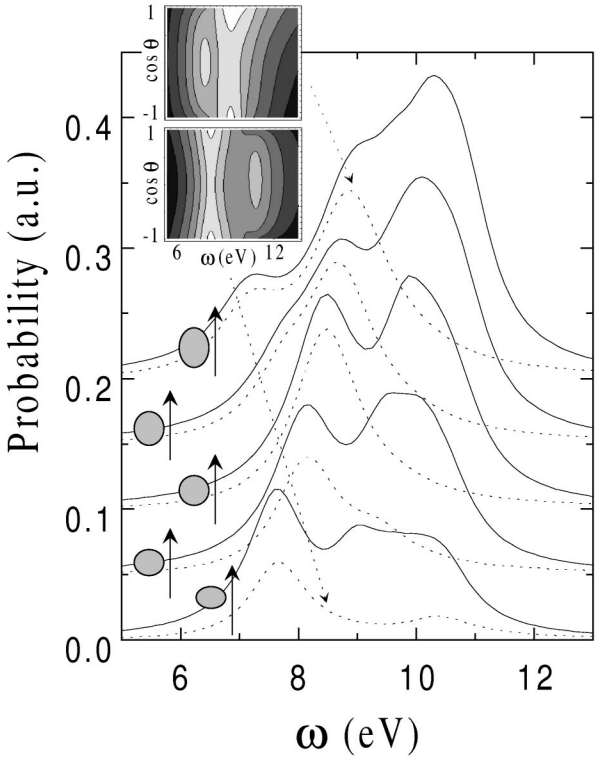

FIG. 4. Loss probability (solid curves) and photon-emission probability (broken curves, multiplied by a factor of 3) for a 100-keV electron passing at a distance of 1 nm from the surface of a Al cylindrical ellipsoid. The electron moves parallel to the axis of symmetry, along which the semiaxis of the ellipsoid takes different values ($b = 14$, 12, 10, 8, and 6 nm from top to bottom; see insets). The other semiaxis is 10 nm in all cases. Consecutive curves have been shifted 0.05 a.u. upwards to improve readability. The angular distribution of photon-emission probability is shown in the insets for the extreme cases of $b = 6$ nm and $b = 14$ nm.

plots of Fig. 3 exhibit a preference for emission along the direction of motion of the electron.

The features of both the loss function and the photon-emission probability are very sensitive to the structure of the object along the direction of motion of the electrons, as shown in Fig. 4, where the loss probability (solid curves) and the photon-emission probability (broken curves, multiplied by 3) are represented for ellipsoidal targets with the same circular projection perpendicular to the electron trajectory.

In summary, a formalism has been presented to simulate fully relativistic electron energy loss and electron-induced photon-emission spectra in the presence of arbitrarily shaped dielectrics. Making use of the boundary element method, the three-dimensional solution of Maxwell's equations is reduced to surface-integral equations. Even in small isolated spheres, the electronic damping and radiation losses can be comparable, raising the possibility of direct detection of the latter as a new source of microscopical information on the target. In larger systems or in Cherenkov emission situations, relativistic effects will be even more significant.

We thank the Departamento de Educación del Gobierno Vasco for support to F. J. G. A. and Iberduero SA for a Visiting Professorship to A. H.

[1] R. H. Ritchie, Phys. Rev. **106**, 874 (1957).
[2] P. M. Echenique and J. B. Pendry, J. Phys. C **8**, 2936 (1975).
[3] N. Zabala, A. Rivacoba, and P. M. Echenique, Surf. Sci. **209**, 465 (1989).
[4] T. L. Ferrell and P. M. Echenique, Phys. Rev. Lett. **55**, 1526 (1985).
[5] N. Zabala, A. Rivacoba, and P. M. Echenique, Phys. Rev. B **56**, 7623 (1997).
[6] R. Fuchs, Phys. Rev. B **11**, 1732 (1975).
[7] F. Ouyang and M. Isaacson, Philos. Mag. B **60**, 481 (1989); Ultramicroscopy **31**, 345 (1989).
[8] J. Q. Lu and A. A. Maradudin, Phys. Rev. B **42**, 11 159 (1990).
[9] F. J. García de Abajo and J. Aizpurua, Phys. Rev. B **56**, 15 873 (1997).
[10] E. Kröger, Z. Phys. A **235**, 403 (1970).
[11] R. García-Molina, A. Gras-Martí, A. Howie, and R. H. Ritchie, J. Phys. C **18**, 5335 (1985).
[12] D. M. Purcell and C. R. Pennypacker, Astrophys. J. **186**, 705 (1973).
[13] B. T. Draine and P. J. Flatau, J. Opt. Soc. Am. A **11**, 1491 (1994).
[14] R. Rupping, Z. Phys. D **36**, 69 (1996).
[15] J. B. Pendry and A. MacKinnon, Phys. Rev. Lett. **69**, 2772 (1992); J. B. Pendry and L. Martín-Moreno, Phys. Rev. B **50**, 5062 (1994); F. J. García-Vidal and J. B. Pendry, Phys. Rev. Lett. **77**, 1163 (1996).
[16] N. Ida, *Numerical Modeling for Electromagnetic Non-destructive Evaluation* (Chapman and Hall, New York, 1995).
[17] This new result can be obtained from the scattering of multipoles applied to the sphere. A detailed derivation will be published elsewhere.
[18] Analytical expressions for the phase shifts of homogeneous spheres can be found in K. Ohtaka and M. Inoue, Phys. Rev. B **25**, 677 (1982).
[19] R. Fuchs and K. L. Kliewer, J. Opt. Soc. Am. **58**, 319 (1968).